Range-separated hybrid van der Waals density functionals to describe Cu<inf>2</inf>O<inf>2</inf>-complexes

Chemical Physics Letters 856 (2024) 141589

Contents lists available at ScienceDirect

Chemical Physics Letters

journal homepage: www.elsevier.com/locate/cplett

Research paper

Range-separated hybrid van der Waals density functionals to describe Cu_2O_2-complexes

Carl Frostenson [a], Yingxin Feng [b], Per Hyldgaard [a], Henrik Grönbeck [b,*]

[a] Department of Microtechnology and Nanoscience-MC2, Chalmers University of Technology, Göteborg, SE-412 96, Sweden
[b] Department of Physics and Competence Centre for Catalysis, Chalmers University of Technology, Göteborg, SE-412 96, Sweden

HIGHLIGHTS

- Range-separated hybrid van der Waals density functionals describe activated O_2 in Cu_2O_2 units.
- Chemical and physical bonding can be described without semi-empirical corrections.

GRAPHICAL ABSTRACT

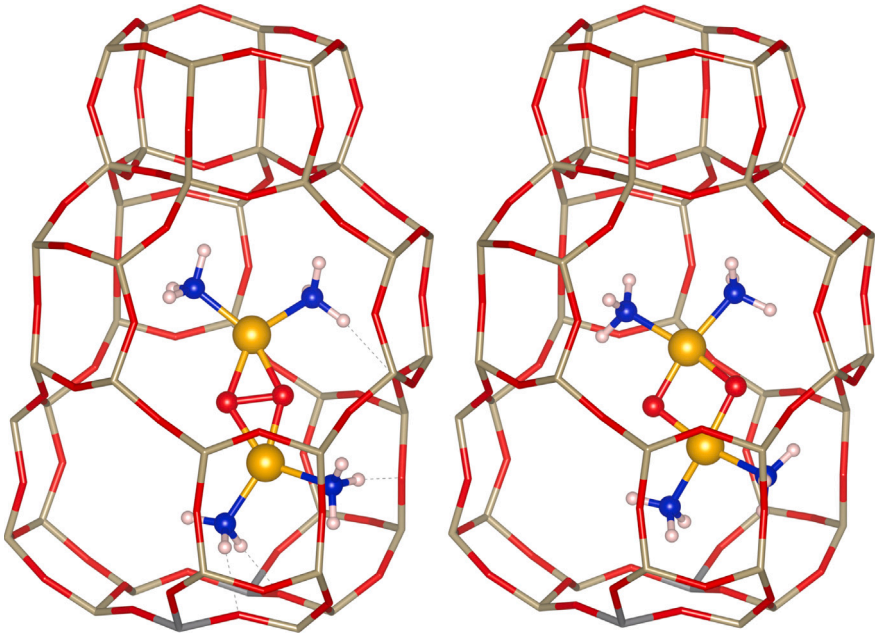

ARTICLE INFO

Keywords:
Density functional theory
Van der waals
Cu-CHA
CuO

ABSTRACT

Dimeric copper centers are commonly used to activate molecular oxygen in enzymatic and heterogeneous catalysis where Cu_2 is embedded in porous structures. Here we evaluate the ability of recently developed range-separated hybrid van der Waals density functionals to describe activated O_2 in a crystal with the Cu_2O_2 unit and in a $[Cu_2(NH_3)_4O_2]^{2+}$ complex embedded in a chabzite zeolite. The electronic and geometrical structure of the Cu_2O_2 unit depends sensitively on the exchange–correlation functional and a sufficiently large amount of short-ranged Fock-exchange is needed to describe the experimentally observed Cu_2O_2 structures.

* Corresponding author.
E-mail addresses: hyldgaar@chalmers.se (P. Hyldgaard), ghj@chalmers.se (H. Grönbeck).

https://doi.org/10.1016/j.cplett.2024.141589
Received 17 June 2024; Received in revised form 28 August 2024; Accepted 29 August 2024
Available online 31 August 2024

1. Introduction

Atomic-level understanding is increasingly becoming an important route for materials development. Control at the atomic-level is experimentally provided by advanced spectroscopy and local imaging probes, whereas electronic structure calculations are used to link materials properties with fundamental understanding of chemical and physical bonds. The advantage of fundamental understanding for materials development has been demonstrated across disciplines where heterogeneous catalysis is but one example [1,2]. Although heterogeneous catalytic reactions often are complex with many simultaneous interactions, it has been possible to successfully describe the performance using first principles-based potential energy diagrams combined with transition state theory and methods for reactions kinetics [2,3]. The potential energy diagrams are within heterogeneous catalysis typically evaluated using Density Functional Theory (DFT) calculations in the generalized gradient approximation (GGA) for exchange–correlation (xc) effects [4,5]. The GGA approach has been very successful to describe catalyst activity and selectivity, in particular, for reactions occurring on metal surfaces and nanoparticles [2].

Nevertheless, there are important cases of molecular adsorption on metal surfaces where GGA fails even when the exchange-functional is fitted to experimental data [6–8] and the performance of GGA-based calculations for reactions over surfaces with electronic gaps, such as oxides, are generally not as convincing as for metallic surfaces. Moreover, it is in many cases crucial to include van der Waals (vdW) forces in a systematic manner [9,10]. One approach is to treat vdW-effects separately as parameterized atom-centered contributions [11–13]. Another approach is to develop truly nonlocal xc-functionals that consider vdW-interactions in the same electron-(spin-)density framework as the other interactions. This has been done within the non-empirical vdW-density functional (vdW-DF) method [9,14–17].

One particular challenge for DFT-based calculations is reactions occurring on metal centers in zeolites where the interactions range from strong ionic and covalent types of bonds to weaker vdW-interactions. Zeolites are aluminosilicates composed of (SiO_4, AlO_4) tetrahedra forming porous cage-structures. The unbalanced charge in AlO_3, is compensated by either a proton in the form of a Brønsted acid site, or metal Fe and Cu cations. The speciation of the metal cations could be dynamic with different types of ligand-stabilized complexes forming during reaction conditions. One example is the formation of $[Cu_2O_2(NH_3)_4]^{2+}$ during selective catalytic reduction of NOx using ammonia as reducing agent (NH_3-SCR) over Cu-exchanged chabazite (Cu-CHA) [18–21]. The complex is during typical reaction conditions floating in the zeolite framework and has experimentally by X-ray absorption spectroscopy been characterized to have a Cu_2O_2 core with a μ-η^2: η^2 (side-on) peroxo structure [22].

The floating state of $[Cu_2O_2(NH_3)_4]^{2+}$ is the result of the combination of ionic, vdW, and steric interactions between the positively charged complex and the negatively charged zeolite framework. The local structure and properties of the Cu_2O_2 core is determined by the Cu-to-O charge transfer, which depends on the localization of Cu $3d$ states. Generally, complexes with the Cu_2O_2 core exist either in the side-on peroxo structure or in a bis(μ-oxo)-configuration, where the O-O bond is broken, see Fig. 1. The computational description of these systems is challenging as has been outlined in wavefunction-based studies of $[Cu_2O_2(NH_3)_4]^{2+}$ by Cramer and co-workers [23]. Isolated Cu_2O_2 complexes in the side-on configuration are open-shell singlet bi-radicals that can have pronounced multireference character [24]. In fact, the side-on-versus-bis energy difference varies dramatically (within 1.7 eV) with the choice of wavefunction method [23]. In Ref. [23] it was suggested that the, so-called, renormalized coupled-cluster approach [25] provides the most reliable results. The renormalized coupled-cluster approach leads to a degeneracy between the side-on and bis-configurations for isolated $[Cu_2O_2(NH_3)_4]^{2+}$, which, however, appears to be in contrast with the experimental observations for complexes embedded in the CHA zeolite [22]. A broad analysis of open-shell biradicals by Gräfenstein, Cremer, and co-workers [24,26] has shown that the use of the global hybrid B3LYP [27,28] for xc-effects can give substantial errors for Cu_2O_2 complexes [23], interestingly, because it reduces the extent of self-interaction errors (SIEs) that exist (and aid!) a GGA description of the isolated systems. [26] It should be noted that wavefunction-based calculations consider gas-phase structures, which are not completely structurally optimized. The global minimum for gas-phase $[Cu_2O_2(NH_3)_4]^{2+}$ is, for example, two separated $[Cu(NH_3)_2]^{+}$ complexes and an O_2 molecule. Moreover, the charge state of the considered systems is fixed to the formal charge state, whereas the $[Cu_2O_2(NH_3)_4]^{2+}$ structure in Cu-CHA is stabilized by an extended embedding environment with anionic counter charges.

A computationally cheap approach to control SIEs is to enforce localization by including a Hubbard-U term (DFT+U) [29]. Within DFT-approaches, and for the extended systems, it has been shown that a Hubbard-U correction or some amount of Fock-exchange in a range-separated hybrid form [30] is required to properly describe the electronic structure of gas-phase $[Cu_2O_2(NH_3)_4]^{2+}$ structures [31]. Moreover, for $[Cu_2O_2(NH_3)_4]^{2+}$ in extended Cu-CHA it has been shown that the preference for the side-on or bis structure depends critically on the choice of functional [32]. In Ref. [32] it was concluded that reasonable accuracy could be obtained at low computational cost by combining the Hubbard-U approach with parameterized vdW-interactions. However, the use of parameterized methods, like Hubbard-U corrections and effective potentials (such as dispersion corrections) for vdW-interactions, are not fully satisfactory. The determination of the U-term is generally ambiguous and the value could change along a reaction path. Limited transferability of parameterized methods could result in false conclusions regarding preferred structures and reaction paths.

In summary, the Cu_2O_2 core is a system that poses several challenges. Questions that arise are: Is it possible to simultaneously (i) secure a balanced inclusion of chemical, ionic and vdW-bonding for embedded Cu_2O_2 units, [32,33] (ii) provide a working DFT description in spite of scatter in performance for wavefunction methods [23], and (iii) avoid excessive electron delocalization by using a fraction of Fock-exchange when the performance of global-hybrid descriptions to counteract delocalization in Cu_2O_2 systems is uncertain [23,24,26]?

The performance of computational methods should ideally be assessed by comparisons to experimental data. The local Cu_2O_2-structure of the $[Cu_2O_2(NH_3)_4]^{2+}$ complex is similar to the structure of biological Cu-centers in enzymes [34,35]. Hemocyanins, tyrosinase, and catechol oxidase are three such enzymes having copper dimers to activate molecular oxygen. Crystals with the Cu_2O_2-motif in an organic matrix have been synthesized and structurally characterized by single-crystal diffraction [36]. Crystals have been synthesized with the Cu_2O_2-unit having both the side-on ($[Cu_2^{II}(O_2^{2-})]^{2+}$) and the bis-configuration ($[Cu_2^{III}(O^{2-})_2]^{2+}$). The O-O bond is retained in the side-on configuration being about 1.4 Å, whereas it is broken in the bis-configuration being about 2.3 Å. The total charge of the complexes is +2, indicating that the formal charge on Cu cations in the two structures is II and III, respectively. The $3d^9$ electronic configuration in the side-on structure gives the possibility of either anti- or ferromagnetic coupling of the spins. The anti-ferromagnetic coupling (singlet) is generally determined to be the preferred spin configuration [31].

In this work, we evaluate newly developed range-separated hybrid van der Waals density functionals for the $[Cu_2O_2(NH_3)_4]^{2+}$ complex in Cu-CHA and a crystal with the Cu_2O_2 motif. The new functionals, termed vdW-DF-ahcx [17] (AHCX) and vdW-DF2-ahbr [10] (AHBR), constitute controlled updates of GGA [17]. We go beyond previous studies of gas-phase biradical analogues as we consider embedded Cu_2O_2 units, which are structurally optimized and where the charge transfer between the Cu_2O_2 unit and the embedding environment is not predetermined. Using the AHCX and AHBR functionals, we correctly describe the experimentally determined preference for the side-on configuration. In addition to the Cu_2O_2 systems, we present, as

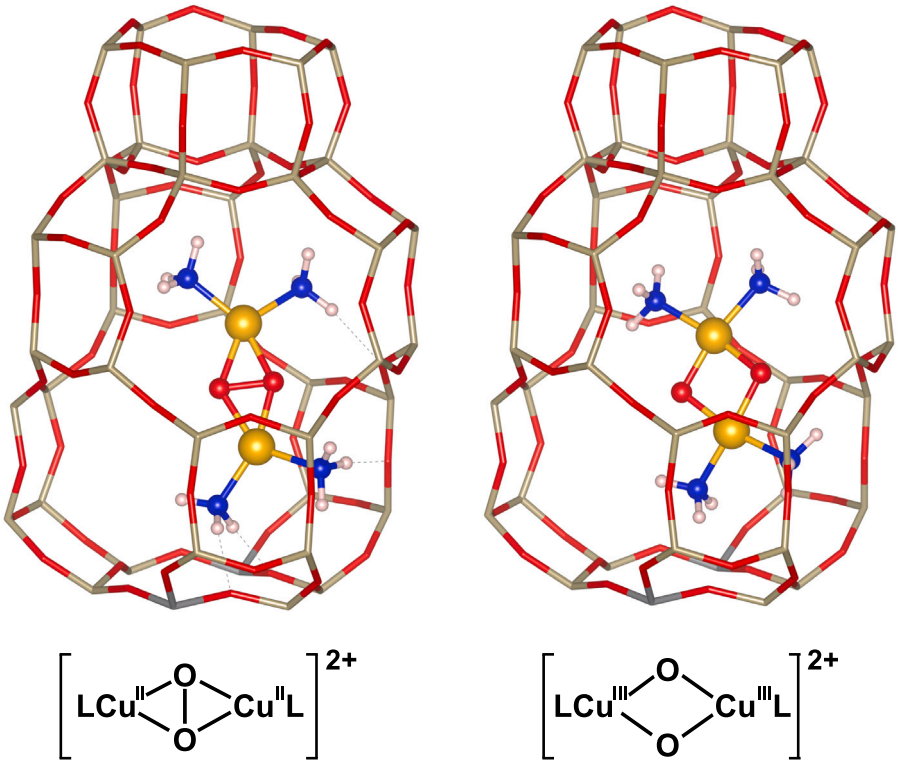

Fig. 1. (Top panel) Side-on peroxo $[Cu_2^{II}(O_2^{2-})]^{2+}$ and bis(μ-oxo) $[Cu_2^{III}(O^{2-})_2]^{2+}$ complexes in a cage of CHA. (Bottom panel) Sketch of side-on and bis configuration, using "L" to denote the ligands. We consider the Cu_2O_2-complex embedding where each ligand comprises two NH_3 groups.

a benchmark, results for the gas phase CuO dimer. Our work shows that it is possible to describe these challenging systems, from first principles, without empirical corrections and without assumptions regarding charge or spin states.

2. Theory and computational details

The use of range-separated hybrid vdW-DFs [10,17] for embedded Cu_2O_2 units is, in part, motivated by the arguments in Ref. [24] regarding the different impacts SIEs have on DFT calculations [26]. We first note that DFT is, in principle, exact in the sense that there is a formal many-body perturbation theory path to construct a universal xc-energy functional [37,38]. GGAs and vdW-DFs exist that allow for accurate descriptions of both molecular systems and condensed phases [10,39,40]. These GGAs and vdW-DFs are systematic extensions [9] of the local (spin) density approximation [37] (LDA) that, in turn, rests on Slater exchange. This means that the exchange components of such xc-functionals screen the long-range components of Fock-exchange, thereby providing implicit long-ranged correlation effects;[38] The nominal correlation term of GGAs and vdW-DFs exclusively reflects additional effects arising from the electron–electron interaction [9,15,24,37]. The resulting xc-functional permits single-determinant Kohn–Sham DFT descriptions that, for some systems suffers from SIEs and excessive delocalization [10]. The implicit long-range screening in LDA exchange is valuable and is only weakly softened in exchange descriptions of GGAs and vdW-DFs [4,5,41,42]. The long range screening helps GGA and vdW-DF descriptions of bulk systems [9] and many molecule systems [10], because the SIE in LDA mimics long-range nondynamical correlation effects to some, still incompletely characterized, extent [24,26].

A possible drawback of using Kohn–Sham DFT for the considered systems is that this single-determinant approach can likely only serve as an ensemble-state representation [26,43] of the gas-phase open-shell singlet Cu_2O_2 complexes [23]. The advantage is that the considered systems are both extended and open (in a statistical-ensemble sense), which permits net (average) and virtual charge transfers between the Cu_2O_2 units and the embedding environment. The result may be interpreted as an ensemble representation in DFT [26]. Moreover, GGA – for both the isolated [23] and the embedded [32] Cu_2O_2 cases – avoid the dramatic errors that emerge in some wavefunction methods [23,24]. Specifically, both PBE [32] and BLYP [4,28] predict only a small (0.2 eV) preference for the bis configuration of Cu_2O_2 complexes. The near-degeneracy of side-on and bis-configurations in GGA is consistent with the most trusted method of Ref. [23]. Of course, finding even an energy degeneracy [23] is still in conflict with experiments, [22] and methods beyond GGA are clearly needed. Nevertheless, DFT in the electron-gas tradition [9,10,37,38] is a promising framework for this type of problems [24].

To put the discussion of regular (that is, density explicit) vdW-DFs as well as of AHCX and AHBR in a formal framework, we note that the xc-energy $E_{\rm xc}$ is a functional of the electron-density $n(\mathbf{r})$. In non-empirical functionals, such as PBE and vdW-DFs, [5,9,15] it can be expressed as a correction to the mean-field electron Coulomb energy, [17,37,44,45]

$$E_{xc}[n(\mathbf{r})] = \frac{1}{2}\int_{\mathbf{r}}\int_{\mathbf{r}'} \frac{n(\mathbf{r})n_{xc}(\mathbf{r};|\mathbf{r}'-\mathbf{r}|)}{|\mathbf{r}-\mathbf{r}'|}\,. \quad (1)$$

Here $n_{xc}(\mathbf{r};|\mathbf{r}'-\mathbf{r}|)$ denotes the so-called, xc-hole that expresses the tendency for an electron at $\mathbf{r}$ to suppress the electron occupation in a neighborhood, at distance $|\mathbf{r}'-\mathbf{r}|$. The exchange-energy E_x is also defined via Eq. (1), replacing n_{xc} by a physics-motivated exchange-hole $n_x(\mathbf{r};|\mathbf{r}'-\mathbf{r}|)$ approximations with a finite $|\mathbf{r}'-\mathbf{r}|$ range;[17,44] The underlying assumption is that screening cancels the long-ranged interactions that arise in Eq. (1) when n_x is instead approximated at the Fock-exchange level [38]. The difference $n_c \equiv n_{xc} - n_x$ defines the correlation-energy functional $E_c[n(\mathbf{r})]$ that also is approximated in DFT using either the GGA or vdW-DF frameworks [5,9,15].

Among the regular vdW-DFs, we use here the consistent-exchange vdW-DF-cx [42] (CX) and the vdW-DF2-b86r [41] (B86R, also called rev-vdW-DF2) functionals. The CX and B86R have shown good performance for most traditional bulk, layered and surface systems, [10,

Table 1
Comparison of molecular properties for CuO using different exchange–correlation functionals. The calculated properties are binding energy (E_{bind}), Cu-O bond length ($\bar{d}_{Cu-O}$), harmonic wavenumber (ω_e), anharmonic correction to the wavenumber ($\omega_e x_e$), Bader charge (e) and dipole moment (μ).

Functional	E_{bind} (eV)	$\bar{d}_{Cu-O}$ (Å)	ω_e (cm^{-1})	$\omega_e x_e$ (cm^{-1})	Cu (e)	μ (D)
CX	−3.26	1.70	703	22	0.57	4.08
B86R	−3.25	1.70	692	11	0.56	4.00
HSE+D3	−2.66	1.74	623	8	0.59	4.56
$AHCX_{0.20}$	−2.75	1.72	645	10	0.58	4.42
$AHCX_{0.25}$	−2.64	1.73	633	14	0.59	4.51
AHBR	−2.61	1.73	622	4	0.58	4.45
Exp. [47,48]	−2.79	1.72	640.2	4.43	–	4.57

40] for molecular properties, [10] and for molecular crystals [40]. However, the CX and B86 functionals can have issues with electron self-interaction and delocalization errors [10,32].

The recent development of range-separated hybrid vdW-DFs, the AHCX [17] and AHBR [10], extend the logic of the HSE generalization of PBE [30,45]. All three range-separated hydrids provide a rigorous way to mix-in Fock-exchange when using Eq. (1) to define a short-range (SR) E_x^{SR}. For AHCX (AHBR), this is done by analyzing the nature of exchange in CX and in B86R using an analytical-exchange-hole modeling [17,45]. As in HSE06, [30] the cross-over is set by an assumed fixed inverse length-scale and a fraction α of E_x^{SR} is replaced by an efficient Fock-exchange evaluation [10,17,46]. For AHBR (AHCX) we keep the choice of short-range Fock-exchange mixing fixed at the default $\alpha = 0.25$ value (at both 0.20 and 0.25 values, as identified by subscripts).

We have some basic trust in the nonempirical AHCX and AHBR as potential tools to characterize the embedded-Cu_2O_2 systems. Both AHCX and AHBR provide significant progress for molecular barrier accuracy [10], as tested on the GMTKN55 benchmark suite [39]. Some of these barriers are expected to require multi-configuration approaches when described in a wavefunction framework. Furthermore, AHCX and AHBR are good candidates for addressing embedded-Cu_2O_2 units because they limit the inclusion of Fock-exchange to short ranges. They retain the long-ranged correlation effects that are implicitly included in LDA/GGA/vdW-DF exchange [9,38]. They may therefore retain the ability to mimic long-range nondynamic correlation effects, by the mechanism discussed in Refs. [24,26].

All calculations are performed using the QUANTUMESPRESSO (QE) suite [46,49] and nonempirical xc-functionals that includes truly nonlocal correlations. We compare regular [41,42] and new range-separated hybrid vdW-DFs [10,17] with the original range-separated hybrid HSE [30] augmented with semi-empirical dispersion-corrections (Grimme-D3) [12].

We use the optimized norm-conserving Vanderbilt pseudopotentials [50,51] (PP) generated using PBE. [5] The electrons treated in the valence for each element are H(1), N(5), O(6), Al(10), Si(4) and Cu(19). Note that the semi-core states are included in the valence. To allow for a simple comparison with a broad set of earlier AHCX and AHBR benchmarking results, [10,17,40] the valence electrons are described with a plane wave basis set using a very high kinetic energy cutoff of 2180 eV for the Kohn–Sham orbitals and a four times higher energy cutoff for the density.

Gas-phase systems are considered in large cubic cells using only the Γ-point. The k-point integration for the crystal systems are approximated with a finite sampling. Both the zeolite structure and the crystals with the Cu_2O_2-units are modeled with $2 \times 2 \times 2$ meshes centered at the Γ-point. A small Gaussian smearing of 0.013 eV is used to facilitate the convergence of the self-consistent field loop. The electronic structure is considered to be converged when the energy difference between two subsequent steps in the self-consistent cycle is below 2×10^{-7} eV. Structures are optimized using the Broyden–Fletcher–Goldfarb–Shanno (BFGS) algorithm and considered to be converged when the force acting on each atom is smaller than 5×10^{-5} eV/Å.

Vibrational analysis is performed for CuO where the wavenumber is obtained by calculating the total energy of the molecule as a function of Cu-O distance. The harmonic wavenumber (ω_e) is obtained via an harmonic fit to the potential energy curve. The anharmonic wavenumber is calculated by solving the Schrödinger equation for the potential energy curve. The anharmonic corrections ($\omega_e x_e$) are thereafter obtained using the second order expansion of the potential energy curve:

$$E(n) = \omega_e \left(n + \frac{1}{2}\right) - \omega_e x_e \left(n + \frac{1}{2}\right)^2. \quad (2)$$

We compute the energy difference (ΔE_{TS}) between the triplet (E_T) and singlet (E_S) states for Cu_2O_2-complexes by:

$$\Delta E_{TS} = E_T - E_S. \quad (3)$$

The triplet state represents ferromagnetic coupling between two $3d^9$-configurations of the Cu-ions, whereas the singlet state can represent anti-ferromagnetic coupling between the $3d^9$-configurations or a non-magnetic (spin-balanced) state.

3. Results

3.1. CuO molecule

We use the gas-phase CuO molecule as a test case for the description of the Cu-O bond (Table 1). The molecule is considered in a cubic cell with a side of 15.6 Å. The calculations use a Makov-Payne mono- and dipole correction to decouple periodic images [52]. The binding energy is calculated as the total energy difference between CuO and atomic Cu and O in doublet and triplet configurations, respectively. The molecule is a doublet with an experimental dissociation energy of 2.79 eV, bond distance of 1.724 Å and harmonic wavenumber of 640.2 cm^{-1} [47].

The CX-functional clearly overestimates the binding energy of the molecule with respect to the experimental value. The overestimation of the bond-strength correlates with a too short bond distance and a too high vibrational wavenumber. The results for the B86R functional are similar to CX. Adding Fock-exchange to the xc-functional has a clear effect on the calculated properties. The binding energy is lowered by about 0.5–0.6 eV, yielding values close to the experimental result. The shape of the potential energy curve is also affected as evidenced by lowering of both ω_e and $\omega_e x_e$. The AHBR functional gives a slightly too low vibrational wavenumber, however, the anharmonic correction is very close to the experimental value.

The better performance of the functionals with short-ranged Fock-exchange is related to a higher degree of electron localization [10]. The Bader charge analysis shows a larger charge separation for the range-separated hybrid functionals than for CX and B86R. Thus, the bonding in the molecule has a higher degree of ionicity with inclusion of some short-ranged Fock exchange. The dipole moment for CuO has been measured to be 4.57 Debye [48] and the calculated dipole moment is close to the experimental value when using the range-separated hybrid functionals. Again, the inclusion of some short-ranged Fock exchange improves accuracy in the description of the charge separation.

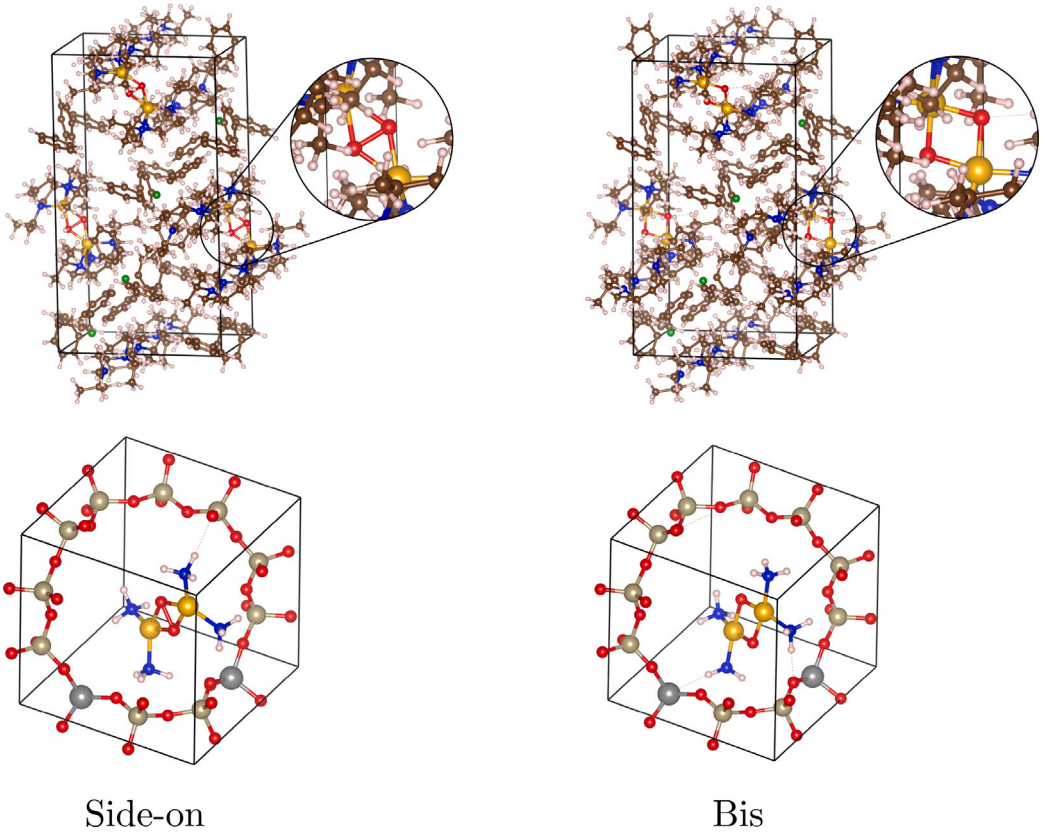

Fig. 2. Unit cells and configurations of embedded Cu_2O_2 complexes for iPr3TACD (top row) and chabazite (bottom row). The set of left and right panels show side-on peroxo and bis Cu_2O_2 motifs or complexes, of which there are one in the chabazite unit cell and two in the crystal unit cell.

3.2. $[Cu_2O_2(NH_3)_4]^{2+}$ in chabazite

The $[Cu_2O_2(NH_3)_4]^{2+}$ complex is a key intermediate formed during NH_3-SCR at low temperatures in the CHA zeolite [21]. It is a challenging system to describe computationally as $[Cu_2O_2(NH_3)_4]^{2+}$ is mobile without chemical bonds to the zeolite framework. The non-directional interaction to the framework results in shallow potential energy surface with many local minima. Here we consider the side-on peroxo $[Cu_2(O_2^{2-})]^{2+}$ and bis(μ-oxo) $[Cu_2(O^{2-})_2]^{2+}$ structures of $[Cu_2O_2(NH_3)_4]^{2+}$, Fig. 2. The side-on peroxo $[Cu_2(O_2^{2-})]^{2+}$ structure has been inferred from X-ray absorption spectroscopy (XANES and EXAFS) [22]. The structure was measured to have Cu-Cu and Cu-O bond lengths of 3.40 ± 0.05 and 1.911 ± 0.009 Å, respectively. The Cu-Cu distance is consistent with a side-on peroxo structure and implies a slightly bent structure with a Cu-O-O-Cu torsion angle of about 150°.

The structures of bis(μ-oxo) and side-on peroxo in CHA are completely relaxed using the CX functional. The differences in cell sizes between the bis and side-on structures are small (see Supplementary Material), which is reasonable given that the copper-complexes are floating in the zeolite cage without directional bonds. The bis-structure is with the CX functional preferred over the side-on peroxo structure by 0.352 eV, which contradicts the experiments [22]. The Cu-Cu distance is 2.715 Å and 3.509 Å in the bis and side-on peroxo structures, respectively. A distance of ~3.50 Å is consistent with the EXFAS report of 3.40 ± 0.05 Å [22]. The corresponding O-O distances are 2.328 Å (bis) and 1.482 Å (side-on peroxo). Moreover, the Cu-O-O-Cu torsion angle is calculated to be 169° (173°) for bis (side-on peroxo).

The CX structure was used to investigate the performance of the other vdW-DF functionals. see Table 2. A complete structural relaxation using Fock-exchange was not possible due the high kinetic energy cutoff in these calculations.

In contrast to the CX-result, the side-on structure is preferred for the functionals including short-ranged Fock-exchange. The exception for $AHCX_{0.20}$ suggests that the amount of Fock-exchange in that case is too small. It is known that the magnetic coupling between the Cu-atoms in di-nuclear complexes is sensitive to the degree of d-electron localization [31]. For the side-on structure, the energy difference between the singlet and triplet states is 1.094 eV for CX, whereas it is about 0.55 eV for the range-separated hybrid functionals. The large ΔE_{TS}-value for CX is a signature of a high degree of delocalization where the spin-states on the two Cu atoms are coupled. The bis-structure is a fully-spin-balanced delocalized singlet with zero magnetic moment for all functionals. The range-separated hybrid descriptions for the side-on structure gives an antiferromagnetic ground state with an absolute magnetic moment of about 0.7 μ_B for the functionals with Fock-exchange. The magnetic moment is slightly lower for $AHCX_{0.20}$, which is a consequence of the lower degree of d^9 localization. We also note that the singlet ground state of the side-on structure for CX is spin-balanced, that is, without any magnetic moment on the Cu ion.

3.3. Crystal with the Cu_2O_2-motif

Metalloproteines with oxygen bound to di-copper centers have been synthesized with both bis- and side-on peroxo structures [34,35]. The preferred structure depends on the nature of the ligand. Here we investigate 1,4,7-iPr-1,4,7-triazacyclodecane (iPr3TACD/peroxo), where the crystal contains two units of $[Cu_2O_2(N_3C16H35)_2]^{2+}$, $(B(C_6H_5)_4^-)_2$, (Fig. 2). The Cu_2O_2 core has by single crystal diffraction been measured to have a side-on structure [36].

The iPr3TACD/peroxo crystal is structurally optimized in CX (Table 3) and the energetics is evaluated in CX and three functionals with a part of Fock-exchange, Table 4. The calculations reveal that the bis-configuration is preferred by 0.34 eV in the CX functional. The situation is different for the range-separated hybrid functionals. The HSE+D3 functional shows a clear preference for the side-on configuration by 0.43 eV and also the $AHCX_{0.25}$ and AHBR have preferences for

Table 2
Analysis of the bis (μ-oxo) and side-on peroxo structures in CHA using the structure calculated in CX. The notation in "Functional" is: (the applied functional)/(functional used for the structure). ΔE is the energy difference between the two structures (eV). m is the absolute magnetic moment on one Cu atom (μ_B). ΔE_{TS} is the energy difference between the singlet and triplet state of the side-on structure (eV). $E^{c,nl}_{embed}$ is the non-local correlation part of the embedding energy (see Eq. (4)) calculated either with charged or neutral fragments.

Functional	Structure	ΔE	m	ΔE_{TS}	$E^{c,nl}_{embed}$	$E^{c,nl}_{embed}$(neutral)
CX/CX	bis	0	0	–	−2.178	−2.429
	side-on	0.352	0	1.094	−2.524	−2.445
HSE+D3/CX	bis	0	0	–	−1.889	−2.168
	side-on	−0.324	0.76	0.540	−1.818	−2.124
AHCX/$CX_{0.20}$	bis	0	0	–	−2.408	−2.427
	side-on	0.010	0.64	0.553	−2.482	−2.422
AHCX/$CX_{0.25}$	bis	0	0	–	−2.400	−2.428
	side-on	−0.155	0.74	0.558	−2.468	−2.419
AHBR/CX	bis	0	0	–	−1.688	−1.562
	side-on	−0.201	0.73	0.560	−1.739	−1.682

Table 3
Structural parameters for the Cu_2O_2 unit in the iPr3TACD crystal relaxed in the CX functional together with experimental single crystal X-ray diffraction data.

	Structure	CX	Experiment [36]
d_{Cu-Cu}	bis	2.86	–
	side-on	3.57	3.52
d_{Cu-O}	bis	1.82	–
	side-on	1.93	1.89
d_{O-O}	bis	2.25	–
	side-on	1.48	1.37
ϕ(°)	bis	173	–
	side-on	173	172

Table 4
Energy difference (ΔE) in eV between bis and side-on structures per Cu_2O_2 unit for the iPr3TACD crystal. m is the absolute magnetic moment on one Cu atom (μ_B).

	Structure	CX/CX	HSE+D3/CX	$AHCX_{0.20}$/CX	$AHCX_{0.25}$/CX	AHBR/CX
ΔE	bis	0	0	0	0	0
	side-on	0.34	−0.43	0.06	−0.58	−0.58
m	bis	0	0	0	0	0
	side-on	0	0.85	0	0.83	0.83

the side-on structure. The two structures have similar stability in the $AHCX_{0.20}$ functional.

The preference for the side-on structure for the functionals with Fock-exchange is similar to the Cu_2O_2 complexes in CHA, which is connected to an antiferromagnetic coupling of $3d^9$ configurations in the Cu atoms. The ground state is singlet also for the bis configuration. However, the state is for the bis-configuration completely spin balanced owing to the delocalized character of the states. A spin balanced solution is obtained for the side-on structure also for the CX functional and $AHCX_{0.20}$. Again, the absence of magnetic moments in the AHCX0.20 characterization suggests that the excessive delocalization results in an incorrect prediction of the preferred structure.

4. Discussion

The interaction energy between the $[Cu_2O_2(NH_3)_4]^{2+}$ complex and the CHA cage originating from non-local correlation ($E^{c,nl}_{embed}$) can be evaluated as:

$$E^{c,nl}_{embed} = E^{nl}_c(\text{system}) - E^{nl}_c(CHA^{2-}) - E^{nl}_c(Cu_2O_2(NH_3)^{2+}_4)\,. \quad (4)$$

Here, the non-local correlation energy is calculated for the total system, the CHA cage without the complex and the gas phase $Cu_2O_2(NH_3)_4]^{2+}$ complex. The CHA contains two Al-sites, which means that it formally is doubly negatively charged. $E^{c,nl}_{embed}$ is −2.524 eV for the side-on configuration using the CX-functional and −1.739 eV for AHBR (Table 2).

We can compare the nonlocal-correlation embedding-energies of the range-separated hybrid vdW-DFs to the corresponding energy difference, −1.818 eV, that originates from beyond-LDA correlation-energy in the HSE+D3 functional. We note that the vdW-dominated embedding energy is larger for the side-on structure than for the bis structure using the vdW-functionals, whereas it is smaller for HSE+D3. The vdW-DFs describe the vdW-interaction though an explicit xc-functional, which permits a spatially resolved analysis of binding [9], making it possible to identify the origin of the interactions. Fig. 3 (left) shows the non-local energy density difference for the $[Cu_2O_2(NH_3)_4]^{2+}$ complex in CHA considering charged fragments with the CX-functional. The energy density is given in a plane through the Cu_2O_2 unit and shows that the main contribution to the vdW-interaction is the NH_3-ligands, although also one of the oxygen atoms in O_2^{2-} contributes.

Fig. 3 (right panel) show the non-local embedding energy for the case where the fragments are treated in neutral charge states:

$$E^{c,nl}_{embed}(\text{neutral}) = E^{nl}_c(\text{system}) - E^{nl}_c(CHA) - E^{nl}_c(Cu_2O_2(NH_3)_4)\,. \quad (5)$$

The differences in the $E^{c,nl}_{embed}$ for the two treatments of the charges is limited (Table 2). However, comparing the two panels in Fig. 3 shows significant local consequences of the charge states in the nonlocal-correlation description, yielding for example, an erroneous enhancement of the energy density on the oxygen atoms. The vdW-DFs mapping ability helps us to discuss details in the vdW-contribution to the embedding energy.

A correct evaluation of the balance between ionic charge-transfer and vdW-interactions [33] is crucial for a wide range of applications, where electrocatalytic reactions is one important example. For our case of embedded Cu_2O_2 complexes, there is a crucial balance between the chemical Cu-O bond, which depend on the net charge localization at the Cu $3d$, and the weaker vdW interactions. In a HSE+D3 calculation of the embedding energy, the D3-component is not set up to reflect the impact of charging on that balance. Moreover, the AHCX and AHBR are designed to prevent excessive electron delocalization, see, for example, Table 4. We therefore place a higher trust in AHCX and AHBR to simultaneously account for chemical bonding and vdW-binding in cases of partly unknown charge transfer.

Finally, it is interesting to contrast the nature of the present plane-wave-DFT results obtained for embedded $[Cu_2(NH_3)_4O_2]^{2+}$ in extended systems (without predefined charge state) with that of previous wavefunction-based studies of isolated (fixed-charge) systems [23]. The wavefunction-based studies describe a pure molecular $\langle S^2\rangle = 0$ singlet configuration. However, the expected spin–singlet configuration of the Cu_2O_2-unit [23,24] (in the favorable side-on configuration) should be viewed as a regular anti-ferromagnetic materials problem because there is charge transfer between the Cu_2O_2 complex and the extended CHA zeolite. Accordingly, (and in contrast to the wavefunction-based studies) we avoid enforcing any constraints on the charge or spin state.

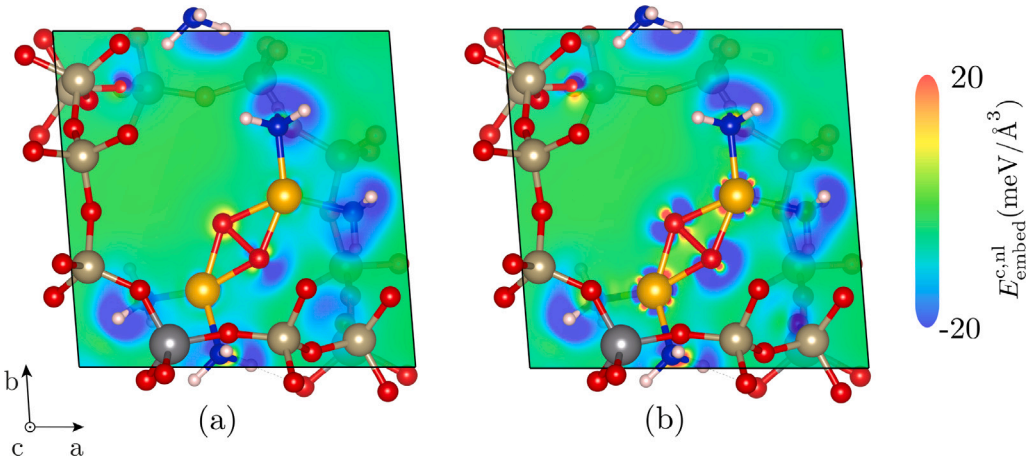

Fig. 3. Non-local correlation energy density evaluated with the CX-functional with charged fragments (left) and neutral fragments (right).

The observation that the isolated Cu_2O_2 system is a biradical that requires a multiconfigurational analysis [23,24] means that we are likely providing a, so-called, ensemble representation in the DFT approach [26]. However, that is desired as we compare with experiments performed on extended matter.

We note that the finding in Ref. [23] for molecular $[Cu_2O_2(NH_3)_4]^{2+}$ that GGA predict the bis-structure to be preferred over the side-on structure agrees with our CX calculations for the extended-system with $[Cu_2O_2(NH_3)_4]^{2+}$ in CHA. Moreover, our finding that the use of a range-separated hybrid form (AHCX/AHBR/HSE+D3) reverses the energy preference is consistent with the observations made for a global hybrid in Ref. [23]. However, as we limit the inclusion of Fock-exchange to short-range effects, we avoid potentially dramatic shifts in the configuration preference [23]. For our extended-system focus, we find that range-separated hybrid functionals provides a controlled change in the charge delocalization among the pair of Cu atoms in the side-on case and, thus, a spin polarization in the Cu_2O_2 antiferromagnets. It is gratifying that AHCX and AHBR not only restores the expected qualitative features (side-on preference and spin polarization) but also provides predictions that can be quantitatively compared to experiments.

5. Conclusions

We have explored recently developed range-separated hybrid van der Waals density functionals to describe activated O_2 in a Cu_2O_2 unit embedded either in a CHA zeolite or in an organic crystal. In addition, the gas phase CuO dimer is considered for reference. The embedded Cu_2O_2 motif is challenging for DFT-based calculations as it requires a proper description of $3d$-localization in the Cu-O bond simultaneously with an account of the weak embedding energy supplied by the zeolite or organic matrix. We find that the electronic and geometrical structure of the Cu_2O_2 unit depends sensitively on the treatment of the exchange and that a sufficiently large amount of Fock-exchange is needed to obtain the experimentally observed structures. The successful description of the Cu_2O_2 structures with a van der Waals density functional demonstrates the possibility to simultaneously model chemical and physical bonds without semi-empirical corrections.

CRediT authorship contribution statement

Carl Frostenson: Writing – original draft, Visualization, Investigation. **Yingxin Feng:** Writing – original draft, Investigation. **Per Hyldgaard:** Writing – review & editing, Supervision, Conceptualization. **Henrik Grönbeck:** Writing – review & editing, Supervision, Conceptualization.

Declaration of competing interest

The authors declare the following financial interests/personal relationships which may be considered as potential competing interests: Henrik Grönbeck reports financial support was provided by Swedish Research Council and the Swedish Energy Agency. Per Hyldgaard reports financial support was provided by Swedish Foundation for Strategic Research and the Swedish Research Council. If there are other authors, they declare that they have no known competing financial interests or personal relationships that could have appeared to influence the work reported in this paper.

Data availability

Data will be made available on request.

Acknowledgment

We acknowledge financial support from the Swedish Research Council (VR) through grants 2018-03964 and 2022-03277, from the Swedish Foundation for Strategic Research (SSF) through grant IMF17-0324, and the Swedish Energy Agency (47110-1). The Competence Centre for Catalysis (KCK) is hosted by Chalmers University of Technology and financially supported by the Swedish Energy Agency (52689-1) and the member companies Johnson Matthey, Perstorp, Powercell, Preem, Scania CV, Umicore and Volvo Group. The authors also acknowledge computer allocations from the Swedish National Infrastructure for Computing under contracts SNIC2021-3-18, SNIC 2022-3-16 and NAISS 2023/3-29, and from the Chalmers Centre for Computing, Science and Engineering (C3SE).

Supplementary material

Supplementary material related to this article can be found online at https://doi.org/10.1016/j.cplett.2024.141589.

Description of the used pseudo-potentials. Bond dissociation energies for $[Cu(NH_3)_x]^+ \longrightarrow NH_3 + Cu(NH_3)_{x-1}]^+$ and charge analysis for $[Cu(NH_3)_x]^+$. Relaxed unit cell for 1,4,7-iPr-1,4,7-triazacyclodecane (iPr3TACD).

References

[1] J.K. Nørskov, T. Bligaard, J. Rossmeisl, C.H. Christensen, Nature Chem. 1 (2009) 37–46.
[2] B.W.J. Chen, L. Xu, M. Mavrikakis, Chem. Rev. 121 (2021) 1007–1048.

[3] M. Jørgensen, H. Grönbeck, ACS Catal. 9 (2019) 8872–8881.
[4] A.D. Becke, J. Chem. Phys. 85 (1986) 7184–7187.
[5] J.P. Perdew, K. Burke, M. Ernzerhof, Phys. Rev. Lett. 77 (1996) 3865–3868.
[6] J.J. Mortensen, K. Kaasbjerg, S.L. Frederiksen, J.K. Nørskov, J.P. Sethna, K.W. Jacobsen, Phys. Rev. Lett. 95 (2005) 216401.
[7] J. Wellendorff, K.T. Lundgaard, A. Møgelhøj, V. Petzold, D.D. Landis, J.K. Nørskov, T. Bligaard, K.W. Jacobsen, Phys. Rev. B 85 (2012) 235149.
[8] N. Gerrits, S.V. Egidius W. F. Smeets, A.D. Powell, K. Doblhoff-Dier, G.-J. Kroes, Phys. Chem. Lett. 11 (2020) 10552.
[9] P. Hyldgaard, Y. Jiao, V. Shukla, J. Phys.: Condens. Matter. 32 (2020) 393001.
[10] V. Shukla, Y. Jiao, J.-H. Lee, E. Schröder, J.B. Neaton, P. Hyldgaard, Phys. Rev. X 12 (2022) 041003.
[11] X. Wu, M.C. Vargas, S. Nayak, V. Lotrich, G. Scoles, J. Chem. Phys. 115 (2001) 8748–8757.
[12] S. Grimme, S. Ehrlich, L. Goerigk, J. Comput. Chem. 132 (2010) 154104.
[13] M. Kim, W.J. Kim, T. Gould, E.K. Lee, S. Lebeque, H. Kim, J. Am. Chem. Soc. 142 (2020) 2346.
[14] M. Dion, H. Rydberg, E. Schröder, D.C. Langreth, B.I. Lundqvist, Phys. Rev. Lett. 92 (2004) 246401.
[15] K. Berland, V.R. Cooper, K. Lee, E. Schröder, T. Thonhauser, P. Hyldgaard, B.I. Lundqvist, Rep. Progr. Phys. 78 (2015) 066501.
[16] T. Thonhauser, S. Zuluaga, C.A. Arter, K. Berland, E. Schröder, P. Hyldgaard, Phys. Rev. Lett. 115 (2015) 136402.
[17] V. Shukla, Y. Jiao, C.M. Frostenson, P. Hyldgaard, J. Phys.: Condens. Matter. 34 (2022) 025902.
[18] P. Vanelderen, J. Vancauwenbergh, B. Sels, R. Schoonheydt, A. Coord. Chem. Rev. 257 (2013) 483–494.
[19] L. Chen, H. Falsig, T. Janssens, H. Grönbeck, J. Catal. 358 (2018) 179–186.
[20] Y. Feng, X. Wang, T.V.W. Janssens, P.N.R. Vennestrøm, J. Jansson, M. Skoglundh, H. Grönbeck, ACS Catal. (2021) 14395–14407.
[21] T.V.W. Janssens, E. Borfecchia, K. Lomachenko, H. Grönbeck, G. Berlier, ChemCatChem (2024) http://dx.doi.org/10.1002/cctc.202400384, Preprint.
[22] C. Negri, T. Selleri, E. Borfecchia, A. Martini, K.A. Lomachenko, T.V.W. Janssens, M. Cutini, S. Bordiga, G. Berlier, J. Am. Chem. Soc. 142 (2020) 15884–15896.
[23] C. Cramer, M. Włoch, P. Piecuch, C. Puzzarini, L. Gagliardi, J. Phys. Chem. A 110 (2006) 1991–2004.
[24] J. Gräfenstein, E. Kraka, M. Filatov, D. Cremer, Int. J. Mol. Sci. 3 (2002) 360–394.
[25] K. Kowalski, P. Piecuch, J. Chem. Phys. 113 (2000) 18.
[26] J. Gräfenstein, D. Cremer, Mol. Phys. 103 (2005) 279–308.
[27] A.D. Becke, J. Chem. Phys. 98 (1993) 5648.
[28] C. Lee, W. Yang, R.G. Parr, Phys. Rev. B 37 (1988) 785.
[29] V.I. Anisimov, J. Zaanen, O.K. Andersen, Phys. Rev. B 44 (1991) 943–954.
[30] J. Heyd, G.E. Scuseria, M. Ernzerhof, J. Chem. Phys. 124 (2006) 219906.
[31] R. Valero, R. Costa, I.d.P.R. Moreira, D.G. Truhlar, F. Illas, J. Chem. Phys. 128 (2008) 114103.
[32] L. Chen, T.V.W. Janssens, H. Grönbeck, Phys. Chem. Chem. Phys. 21 (2019) 10923–10930.
[33] K. Berland, C.A. Arter, V.R. Cooper, K. Lee, B.I. Lundqvist, E. Schröder, T. Thonhauser, P. Hyldgaard, J. Chem. Phys. 140 (2014) 18A539.
[34] L. Mirica, X. Ottenwaelder, T. Stack, Chem. Rev. 104 (2004) 1013–1046.
[35] E. Solomon, D. Heppner, E. Johnston, J. Ginsbach, J. Cirera, M. Qayyum, M. Kieber-Emmons, C. Kjaergaard, R. Hadt, L. Tian, Chem. Rev. 114 (2014) 3659–3853.
[36] B. Lam, J. Halfen, V. Young, J. Hagadorn, P. Holland, A. Lledós, L. Cucurull-Sánchez, J. Novoa, S. Alvarez, W. Tolman, Inorg. Chem. 39 (2000) 4059–4072.
[37] O. Gunnarsson, B.I. Lundqvist, Phys. Rev. B 13 (1976) 4274–4298.
[38] D.C. Langreth, J.P. Perdew, Phys. Rev. B 15 (1977) 2884–2901.
[39] L. Goerigk, A. Hansen, C. Bayer, S. Ehrlich, A. Najibi, S. Grimme, Phys. Chem. Chem. Phys. 19 (2017) 32184.
[40] C.M. Frostenson, E.J. Granhed, V. Shukla, P.A.T. Olsson, E. Schröder, P. Hyldgaard, Electron. Struct. 4 (2022) 014001.
[41] I. Hamada, Phys. Rev. B 89 (2014) 121103(R).
[42] K. Berland, P. Hyldgaard, Phys. Rev. B 89 (2014) 035412.
[43] A. Harju, E. Räsänen, H. Saarikoski, M.J. Puska, R.M. Nieminen, K. Niemelä, Phys. Rev. B 69 (2004) 153101.
[44] J.P. Perdew, K. Burke, Y. Wang, Phys. Rev. B 54 (1996) 16533–16539.
[45] T.M. Henderson, B.G. Janesko, G.E. Scuseria, J. Chem. Phys. 128 (2008) 194105.
[46] I. Carnimeo, S. Baroni, P. Giannozzi, Electron. Struct. 1 (2019) 015009.
[47] K.P. Huber, G. Herzberg, Molecular Spectra and Molecular Structure, Springer, 1979, http://dx.doi.org/10.1007/978-1-4757-0961-2.
[48] X. Zhuang, S.E. Frey, T.C. Steimle, J. Chem. Phys. 132 (2010).
[49] P. Giannozzi, O. Andreussi, T. Brumme, O. Bunau, M. Buongiorno Nardelli, M. Calandra, R. Car, C. Cavazzoni, D. Ceresoli, M. Cococcioni, N. Colonna, I. Carnimeo, A. Dal Corso, S. de Gironcoli, P. Delugas, R.A. DiStasio Jr., A. Feretti, A. Floris, G. Fratesi, G. Fugalio, R. Gebauer, U. Gerstmann, F. Giustino, T. Gorni, J. Jia, M. Kawamura, H.-Y. Ko, A. Kokalj, E. Küçükbenli, M. Lazzeri, M. Marseli, N. Marzari, F. Mauri, N.L. Nguyen, H.-V. Nguyen, A. Otero-de-la Roza, L. Paulatto, S. Poncé, D. Rocca, R. Sabatini, B. Santra, M. Schlipf, A. Seitsonen, A. Smogunov, I. Timrov, T. Thonhauser, P. Umari, N. Vast, X. Wu, S. Baroni, J. Phys.: Condens. Matter. 29 (2017) 465901.
[50] D.R. Hamann, Phys. Rev. B 88 (2013) 085117.
[51] M. Schlipf, F. Gygi, 196 (2015) 36–44.
[52] G. Makov, M.C. Payne, Phys. Rev. B 51 (1995) 4014.